Theoret. Chim. Acta (Berl.) 42, 47–65 (1976)

THEORETICA CHIMICA ACTA

Theoretical Study of the Electronic Structure of Diazomethane

I. The Dissociation Process $CH_2N_2 \rightarrow CH_2 + N_2$ in Point Group C_{2v} Symmetry

Jacques Lievin and Georges Verhaegen

Laboratoire de Chimie Physique Moléculaire, Université Libre de Bruxelles, Faculté des Sciences, Avenue F.D. Roosevelt, 50, B-1050 Brussels, Belgium

Ab initio calculations of the dissociation process $CH_2N_2 \rightarrow CH_2 + N_2$ are presented. Calculations were made on the ground $^1A_1$ state as well as on the first few excited states ($^3B_1$, $^1B_1$, $^1A_1^*$) necessary to the description of the dissociation mechanism in point group C_{2v} symmetry. The variation of energy was determined as a function of the parameters R_{CH}, R_{NN} and θ_{HCH} at several R_{CN} values. Most results were obtained by using a basis set of Gaussian lobe functions contracted to "double-zeta" accuracy. A few calculations were made with the addition of polarization functions on all centers. The equilibrium geometry of the ground state, determined from coupled quadratic equations in the molecular parameters, is in satisfactory agreement with experimental values. The dissociation paths on the potential energy surfaces were determined. The locus of intersection points of the two $^1A_1$ states is described; the avoided crossing of the two potential surfaces was determined from CI calculations based on an "intermediate" Hamiltonian. The geometric and electronic rearrangements due to dissociation as well as the bonding characteristics of the orbitals are discussed.

The dissociation energy of the molecule ($D_0^0(CH_2N_2)$) is calculated to be 0.91 eV.

Finally, the term energy of the $^1A_1$ state of CH_2 is predicted to be 0.49 eV.

Key words: Diazomethane, dissociation of ~

1. Introduction

Diazomethane and related isomers are important species in organic chemistry as they are prime producers of the methylene radical. For this reason, diazomethane finds wide use in organic reactions [1]. Although the chemical properties of the compound are rather well known experimentally, little is known concerning the dissociation mechanism of the molecule to yield methylene and nitrogen.

Theoretically, the molecule has been studied only in its ground state. Snyder and Basch [2] report total energies for diazomethane and diazirine at their equilibrium geometries. Hart [3], using moderately sized basis sets has calculated a series of isomers of the molecule. Leroy and Sana [4] with small and medium-sized basis sets have derived an equilibrium geometry and, by use of localized orbitals, have studied the electronic structure around this geometry. These authors have also derived the enthalpy of formation of the molecule.

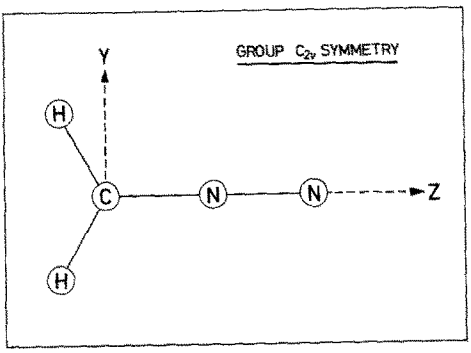

Fig. 1. Geometry and Cartesian coordinates of CH_2N_2

We propose to study the dissociation mechanism of diazomethane to form CH_2 and N_2 products. In this work the dissociation mechanism will be determined in the limiting case of point group C_{2v} symmetry; in subsequent work [5], the symmetry requirements of this group will be relaxed, and the dissociation process will be investigated in point group C_S symmetry more in conformity to expectations according to the Woodward-Hoffmann rules [6].

2. Methods of Calculation

2.1. Geometry

Although CH_2N_2 has a wide variety of isomers, some stable and others presumably unstable [3], this work is devoted to the isomer diazomethane only. Fig. 1 shows the molecule schematically as well as the system of axes adopted in all calculations. Four structural parameters were varied extensively ($R_{CH_1} \equiv R_{CH_2} \equiv R_{CH}, R_{CN}, R_{NN}$ and θ_{HCH}) in order to determine the equilibrium geometry of the molecule as well as the C_{2v} dissociation path. Tables 3 and 4 give a partial list of the geometries considered[1].

2.2. Electronic Configurations and States

According to previous calculations [7], the first few electronic configurations and states of CH_2 are, in order of increasing energy:

$$^3B_1 : (1a_1)^2(2a_1)^2(1b_2)^2(3a_1)(1b_1)$$

$$^1A_1 : (1a_1)^2(2a_1)^2(1b_2)^2(3a_1)^2$$

$$^1B_1 : \text{same as } ^3B_1$$

$$\left\{ \begin{array}{l} ^1A_1^* : (1a_1)^2(2a_1)^2(1b_2)^2(1b_1)^2 \\ ^1\Sigma_g^+ : (1\sigma_g)^2(2\sigma_g)^2(1\sigma_u)^2(1\pi_u)^2 \end{array} \right\}$$

the $^1A_1^*$ state being supposedly linear [7] (in agreement with the present findings).

[1] Due to lack of space, some calculated points were omitted from this list: these include the 13 points necessary to the calculation of the equilibrium properties of the ground state, as well as some other calculated points on CH_2 and N_2.

The first four levels of the dissociation products involve the four CH_2 states above and the ground $^1\Sigma_g^+$ state of N_2[2] corresponding to configuration:

$$^1\Sigma_g^+ : (1\sigma_g)^2(1\sigma_u)^2(2\sigma_g)^2(2\sigma_u)^2(1\pi_u)^4(3\sigma_g)^2$$

In point group C_{2v}, this state and configuration become:

$$^1A_1 : (1a_1)^2(2a_1)^2(3a_1)^2(4a_1)^2(1b_2)^2(1b_1)^2(5a_1)^2,$$

and if one couples the configurations and states of CH_2 and N_2, one obtains in order of increasing energy, the configurations and states (for R_{CN} large):

$$^3B_1 : (1-6)(a_1)^2(1b_2)^2(1b_1)^2(7a_1)^2(2b_2)^2(8a_1)(2b_1) \quad (A)$$

$$^1A_1 : (1-6)(a_1)^2(1b_2)^2(1b_1)^2(7a_1)^2(2b_2)^2(8a_1)^2 \quad (B)$$

$$^1B_1 : \text{same as } ^3B_1$$

$$^1A_1 : (1-6)(a_1)^2(1b_2)^2(1b_1)^2(7a_1)^2(2b_2)^2(2b_1)^2 \quad (C)$$

Previous studies [4] have shown that the ground state of CH_2N_2 (R_{CN} equilibrium is the $^1A_1$ state corresponding to configuration (*C*). Therefore one expects that, in C_{2v} symmetry, this state will intersect the three others.

Of particular interest is the intersection of the two $^1A_1$ states and the study of their avoided crossing. If, as it is the case in the present study, the symmetry requirements are not relaxed, the lower adiabatic $^1A_1$ state will change configuration as R_{CN} increases going from $\ldots(2b_1)^2$ to $\ldots(8a_1)^2$, thereby probably giving rise to a barrier in the corresponding potential energy surface.

In the following, configurations (A), (B) and (C) will be investigated. For the sake of clarity, the $^1A_1$ state of configuration (B) will be written $^1A_1^*$.

2.3. Programs and Calculations

The set of programs used in this work was developed by Whitten and his collaborators. It includes a program which calculates the necessary multicentric integrals over a Gaussian lobe basis set, a program which classifies these integrals according to their symmetry properties, an SCF program, a program which calculates the transformed molecular integrals, and finally a CI program.

The only modification which was made to this set of programs for the present work is the introduction of a decelerating factor in the open-shell part of the SCF program. The effect of this type of factor is to reduce the variation in the one-electron density matrix between two successive iterations. This has for result of accelerating greatly the convergence of the calculations whenever oscillations occur. In the particular cases studied here, important oscillations were found between the 1*s* orbitals of the two N atoms which are quasi-degenerate.

Separate SCF calculations were carried out for the $^3B_1$, $^1A_1$ and $^1A_1^*$ states; the energies of the $^1B_1$ state were obtained from the SCF results of the iso-configurational $^3B_1$ state[3]. The non-crossing of the two $^1A_1$ states was determined from 2 x 2 CI calculations as described below (Sect. 3).

---

[2] The first excited state of N_2 lies more than 6 eV above the ground state [8].

[3] $E(^1B_1) = E^{SCF}(^3B_1) + 2K_{8a_1 2b_1}$. A test on the analogous $^1B_1$ state of CH_2 shows that this approximation is valid within 0.002 a.u.

Table 1. Previous *ab initio* results (a.u.) and basis sets

Ref. No.	Basis Set[a]	$E_{MIN}^{SCF}(CH_2N_2, {}^1A_1)$[b]	Ref.
I	STO-3G (Ref. [9])	− 145.9206	4
II	7s 3p (Ref. [10])	− 147.1857[c]	4
III	LW (533; 3) (Ref. [11])	− 147.2868	3
IV	4-31 G (Ref. [12])	− 147.6055[c]	4
V	(42/2) (Refs. [2, 13, 14])	− 147.7702[c]	2
VI	Whitten 83, 20 (contracted) (Refs. [13, 15])[f]	− 147.5161[d]	L.V.[e]
VII	Whitten 83, 34 (Refs. [13, 15])[f]	− 147.7704	L.V.
VIII	Whitten 83, 49 (Refs. [13, 15])[f]	− 147.7772[d]	L.V.
IX	Whitten 85, 34 (Refs. [13, 16])[f]	− 147.7714[d]	L.V.
X	Whitten 96, 47 (Refs. [13, 15, 17])[f]	− 147.8207[d]	L.V.

[a] References in this column apply to the basis set only.
[b] Unless otherwise indicated, the energies refer to equilibrium geometries as derived from that basis set.
[c] Experimental equilibrium geometry.
[d] Equilibrium geometry obtained from calculations using basis set No. VII.
[e] This work.
[f] First number refers to number of primitives, second to number basis orbitals.

All the calculations were carried out on the CDC 6500 computer of the Université Libre de Bruxelles.

2.4. Basis Sets

In Table 1 are listed a series of results on the ground state of the molecule using different basis sets. The first five entries proceed from previous work, the five last from this work.

Among the literature values, the result of Snyder and Basch [2] only is of comparable accuracy to most of the present results. The other values have been obtained with basis sets inferior to double-zeta quality.

In Table 2 we give a more detailed description of basis sets VI–X. Basis VI, which is totally contracted, has been used only to evaluate the correlation energy of the molecule and of its dissociation products as described in Sect. 2.6.

Basis VII, which is of double-zeta accuracy [18], was used extensively to describe the whole of the potential surfaces. Basis set VIII which is a less contracted combination of the same Gaussian primitives was not used, because the energy increment introduced by the additional relaxation thus introduced (~ 0.007 a.u.) is not sufficient to justify the large increase in computation time ($t(\text{VIII}) \approx 3t(\text{VII})$).

Basis set IX is the same as basis set VII, except that the $1s_H$ basis orbital has 5 instead of 4 lobes, and that a $\sqrt{2}$ scale factor has been introduced for molecular applications. Here again it was judged that the energy difference between sets VII and IX (0.001 a.u.) compared with the respective computer times ($t(\text{IX}) = 1.1\ t(\text{VII})$) did not warrant its extensive use.

The difference between sets X and VII is the addition of polarization functions on all centers: one $3d_{yz}$ and two $3d_{xz}$[4] functions were centered on the carbon and on each of

[4] In point group C_{2v} one has: $3d_{x^2-y^2}, 3d_{z^2} \in a_1$; $3d_{xy} \in a_2$; $3d_{xz} \in b_1$; and $3d_{yz} \in b_2$. Since $3d_{x^2-y^2}$ and $3d_{z^2}$ have maximum probability on the Cartesian axes, they introduce only small polarization effects distinct from that of the $2p_x$, $2p_y$ and $2p_z$ orbitals already present in the basis set. $3d_{xy}$ is discarded because the configurations considered do not contain MO's of a_2 symmetry.

Table 2. Description of basis sets

Center	Type	No. Lobes	Basis Sets[a] VI	VII	VIII	IX	X
C, N	Cont.[b]	3	1	1	1	1	1
	$1s$[b]	4	1	1	2	1	1
	$2s$[b]	3	1	2	3	2	2
	$2p_{x,y,z}$[b]	5	1	2	3	2	2
	$3d_{yz}$[c]	1	–	–	–	–	1
	$3d_{xz}$[c]	2	–	–	–	–	2
H	$1s$[d]	4	1	2	2	–	2
	$1s'$[e]	5	–	–	–	2	–
	$2p_{y,z}$[c]	1	–	–	–	–	1

[a] Numbers in these columns refer to the number of basis orbitals in which the original atomic orbital has been split. When an atomic orbital containing n primitives is split in two basis orbitals, the Gaussian lobe with the lowest exponent becomes one of the basis orbitals, and the $n-1$ remaining primitives, the other.
[b] Ref. [13]. [c] Ref. [17]. [d] Ref. [15]. [e] Ref. [16].

the nitrogen atoms, and one $2p_y$ and $2p_z$ functions were added to the hydrogen set. The exponents and lobe separations of the $3d$ functions on carbon and of the $2p$ functions are taken from the work of Whitten on CH_2O [17]; by analogy the $3d$ functions on nitrogen were chosen with the following parameters:

a) exponent: 0.1758 lobe separation: 0.4131

b) exponent: 0.617 lobe separation: 0.2205

With these additions, the resulting basis set is composed of 96 Gaussian primitives, contracted to 47 basis orbitals. Although the resulting energy is significantly improved with respect to the basis set VII result (0.05 a.u.), the computer time needed for the calculation of one point was too great ($t(X) = 4.5\ t(VII)$) to be able to use this basis set for all calculations. For this reason, SCF results using basis set X were carried out only on two geometries of the ground state and on the dissociation products.

2.5. Determination of the Equilibrium Geometry and Force Constants

Since CH_2N_2 has a total of nine structural parameters (two R_{CH}, R_{CN}, R_{NN}, θ_{HCH}, $\theta_{N_2\text{-}C\text{-}H_2}$ in plane and out of plane, $\theta_{N\text{-}N\text{-}CH_2}$ in plane and out of plane) of which only four were varied in this work, the equilibrium geometry determined here is based on the assumption that the most stable conformation of the molecule is of C_{2v} symmetry ($R_{CH_1} = R_{CH_2}$, and $\theta_{N_2\text{-}C\text{-}H_2} = \theta_{N\text{-}N\text{-}CH_2} = 180°$ in both planes). Another consequence in the presently imposed limitations of geometries is that the force constants calculated here pertain to vibration frequencies of A_1 symmetry only.

To determine the equilibrium geometry, calculated points were fitted to a quadratic expression in each of the four parameters and also containing linear coupling terms

Table 3. Geometries and SCF energies (a.u.) of some calculated points of CH_2N_2 (Basis set VII)

No.	θ_{HCH} (deg.)	R_{CH} (a.u.)	R_{CN} (a.u.)	R_{NN} (a.u.)	$E_{SCF}(^3B_1)$	$E(^1B_1)^a$	$E_{SCF}(^1A_1)$	$E_{SCF}(^1A_1^*)$	ΔE_{CI}^a
1	100.0	2.0385	3.2	2.248	−147.6223	−147.5417	−147.644	−147.4407	±0.0081
2	110.0	2.0385	3.2	2.248			−147.663	−147.4355	
3	121.7	2.0385	3.2	2.248	−147.6285	−147.5563	−147.6803	−147.4245	±0.0052
4	150.0	2.0385	3.2	2.248	−147.6108	−147.5526	−147.69285	−147.3920	±0.0028
5	170.0	2.0385	3.2	2.248			−147.6811		
6	100.0	2.0385	3.2	2.0	−147.6356	−147.5513		−147.4431	
7	100.0	2.0385	3.2	2.1	−147.6614	−147.5781		−147.4529	±0.0084
8	150.0	2.0385	3.2	2.0			−147.7037		
9	150.0	2.0385	3.2	2.1	−147.6290	−147.5688	−147.7102		±0.0029
10	100.0	2.0385	5.0	2.248	−147.7265	−147.6395		−147.6857	
11	110.0	2.0385	5.0	2.248			−147.5819	−147.6860	
12	121.7	2.0385	5.0	2.248	−147.7442	−147.6675	−147.6087	−147.6803	±0.0168
13	150.0	2.0385	5.0	2.248	−147.7401	−147.6760	−147.6503		±0.0313
14	170.0	2.3085	5.0	2.248	−147.7317	−147.6751	−147.6623	−147.6396	±0.0189
15	100.0	2.0385	5.0	2.0	−147.7425	−147.6553		−147.7001	
16	100.0	2.0385	5.0	2.1	−147.7475	−147.6604		−147.7059	±0.0132
17	170.0	2.0385	5.0	2.0			−147.6790		
18	170.0	2.0385	5.0	2.1			−147.6839		
19	170.0	2.0	5.0	2.248			−147.6623		
20	170.0	2.1	5.0	2.248			−147.6601		
21	121.7	2.0385	4.0	2.09			−147.6479	−147.6317	

22	121.7	2.0385	4.1	2.09	−147.7397	−147.6622	−147.6449	−147.6439	±0.0381
23	121.7	2.0385	4.2	2.09			−147.6423	−147.6545	
24	150.0	2.0385	4.8	2.084			−147.6735	−147.6664	
25	150.0	2.0385	4.9	2.084			−147.6729	−147.6703	
26	150.0	2.0385	5.0	2.084	−147.7615	−147.6974	−147.6724	−147.6737	±0.0318
27	100.0	2.0385	3.7	2.095			−147.6143	−147.5936	
28	100.0	2.0385	3.9	2.095			−147.6028	−147.6273	
29	121.7	2.0385	3.8	2.095	−147.7206	−147.6435	−147.6553	−147.6011	±0.0202
30	100.0	2.0385	3.8	2.095	−147.7073	−147.6208	−147.6081	−147.6116	±0.0403
31	80.0	2.0385	3.8	2.095			−147.5413	−147.5995	
32	121.7	2.0385	4.1	2.0			−147.6431	−147.6245	
33	100.0	2.0385	4.1	2.09	−147.7245	−147.6373	−147.5943	−147.6526	±0.0231
34	150.0	2.0385	4.1	2.09	−147.7324	−147.6680	−147.6804	−147.6148	±0.0129
35	121.7	2.0385	4.0	2.248	−147.7129	−147.6361	−147.6255	−147.6136	±0.0332
36	121.7	2.0385	2.8	2.248	−147.538	−147.474			±0.0021
37	121.7	2.0385	6.0	2.248			−147.6044	−147.6955	
38	121.7	2.0385	4.35	2.09	−147.7504	−147.6729	−147.6395	−147.6677	±0.0273

[a] Calculated using orbital energies and transformed molecular integrals of $^3B_1$ SCF calculation (see text for more detail).

between some of them. The expression is:

$$E = a_1 R_{CH}^2 + a_2 R_{CH} + a_3 \theta_{HCH}^2 + a_4 \theta_{HCH} + a_5 R_{CN}^2 + a_6 R_{CN} + a_7 R_{NN}^2 + a_8 R_{NN} + a_9 R_{CH} \theta_{HCH} + a_{10} R_{CH} R_{CN} + a_{11} \theta_{HCH} R_{CN} + a_{12} R_{CN} R_{NN} + a_{13} \quad (1)$$

The first partial derivatives of the energy relative to the four parameters gives the equilibrium geometry and the minimum of energy (E_{MIN}).

Eq. (1) expressed in terms of the symmetry coordinates:

$$\frac{1}{\sqrt{2}}(\Delta R_{CH_1} + \Delta R_{CH_2}) \equiv S_1, \Delta\theta_{HCH} \equiv S_2, \Delta R_{CN} \equiv S_3, \Delta R_{NN} \equiv S_4$$

becomes:

$$\Delta E = k_{CH} S_1^2 + \tfrac{1}{2} k_\theta S_2^2 + \tfrac{1}{2} k_{CN} S_3^2 + \tfrac{1}{2} k_{NN} S_4^2 + \sqrt{2} k_{CH\text{-}\theta} S_1 S_2 + \sqrt{2} k_{CH\text{-}CN} S_1 S_3 + k_{\theta\text{-}CN} S_2 S_3 + k_{CN\text{-}NN} S_3 S_4 .$$

where $\Delta E = E - E_{MIN}$. (2)

Comparison between Eqs. (1) and (2) yields the desired force constants.

If these equations are suitable for representing geometries near the minimum of the potential surface, i.e. for rather small variations of all the parameters, they are inadequate to describe the surfaces along the whole of their dissociation path because of their incorrect asymptotic behaviour in R_{CN}.

A better description is given by an expression of the type:

$$E(Q, R_{CN}) = \sum_{i=1}^{n} [(b_i + b_{n+i} Q + b_{2n+i} Q^2)/R_{CN}^i] + b_{3n+1} + b_{3n+2} Q + b_{3n+3} Q^2 \quad (3)$$

where Q represents R_{CH}, R_{NN} or θ_{HCH}. This equation has a correct asymptotic behaviour in R_{CN} and maintains a quadratic dependence in Q which itself depends on the value of R_{CN}. The coefficients $b_{3n+1}, b_{3n+2}, b_{3n+3}$ are determined for $R_{CN} = \infty$.

Three-dimensional representations of the potential surfaces were obtained from expression (3) with the help of a digital XY plotter (Benson 441) connected to the computer [19].

2.6. Correlation Energies

In view of determining the dissociation energy of CH_2N_2 into CH_2 and N_2 products, the correlation energy of these systems was determined by a semi-empirical method described previously [20].

The underlying idea of this method is to estimate the molecular correlation energy from the atomic (and/or ionic) constituents of the molecule. The charge and electronic states of the constituents are derived from atomic population analyses. The molecular correlation energy is then the sum of the correlation energies of the constituents weighed by their population analysis coefficients [20].

In this work, we have carried out calculations using completely contracted basis sets (basis set VI, see Tables 1 and 2) for this purpose, in order to ensure a one-to-one corre-

Table 4. Geometries, basis sets and SCF energies of some calculated points of CH_2 and N_2 (a.u.) (Basis set VII)

Molecule	State	R (a.u.)	θ (deg.)	E_{SCF}	ΔE_{CI}[a]
CH_2	$^1A_1$	2.0385	121.7	−38.8524	−0.0125
		2.0385	150.0	−38.8269	−0.0196
		2.1	106.0	−38.8585	
CH_2	$^1A_1^*$	2.0385	121.7	−38.7525	
		2.0385	150.0	−38.7959	0.0196
		2.0385	170.0	−38.8094	
CH_2	$^3B_1$	2.0385	121.7	−38.9035	
		2.0385	150.0	−38.9007	
		2.039	132.0	−38.9052	
CH_2	$^1B_1$[a]	2.033	145.9	−38.8399	
		2.0385	121.7	−38.8285	
		2.0385	150.0	−38.8382	
N_2	$^1\Sigma_g^+$	1.948	–	−108.8530	
		2.048	–	−108.8699	
		2.148	–	−108.8667	

[a] See footnote to Table 3.

spondence between the molecular basis orbitals and the atomic orbitals of the constituents. Mulliken's method [21] was used for the atomic population analyses, and the atomic correlation energies were taken from the work of Verhaegen and Moser [22], and Desclaux *et al.* [23].

3. Results and Discussion

3.1. Equilibrium Geometry and Force Constants

The present results are compared to previous work [4] and to experimental values [24, 25] in Table 5.

The calculated values of the equilibrium angle and interatomic distances agree satisfactorily with experiment ($\Delta\theta \approx 3°$ and $\Delta R \approx 0.005$ Å), considering the relatively simple model used here. The particular cases of R_{CN} and R_{NN} deserve closer attention: whereas the sum of the two experimental values agrees well with the corresponding calculated value (2.439 Å, and 2.436 Å respectively), the individual values show a larger discrepancy (~ 0.01 Å). In this specific case, it may well be that the experimental values (obtained from microwave spectroscopy) should be slightly revised, since it is their sum only which seems to be accurately determined [25].

The force constants calculated here also agree relatively well with experiment [24], even in the case of small non-diagonal terms. The fact that the calculated values are systematically high is reasonable and in accord with usual findings using SCF results.

It is also interesting to compare the present results with the calculated values of Leroy and Sana [4] derived from a much smaller basis set (STO-3G, basis I, Table 1). On the whole, their results are of the same general quality as the present ones except for R_{NN}

Table 5. Equilibrium geometry and force constants of $CH_2N_2(^1A_1)$

Property	Experiment[a]	Calculated (Ref. [4])	Calculated (this work)
θ_{HCH} (deg.)	126	121.7	123
R_{CH}(Å)	1.075	1.078	1.080
R_{CN}(Å)	1.300[b]	1.282	1.289
R_{NN}(Å)	1.139[b]	1.189	1.148
$R_{CN}+R_{NN}$(Å)	2.439[b]	2.471	2.436
k_θ (erg/rad^2)	$0.631\cdot10^{-11}$	$3.6\cdot10^{-11}$	$0.801\cdot10^{-11}$
$k_{\theta\text{-CH}}$ (dyn/rad)	–	–	$0.036\cdot10^{-3}$
$k_{\theta\text{-CN}}$ (dyn/rad)	$-0.467\cdot10^{-3}$	–	$-0.583\cdot10^{-3}$
k_{CH} (dyn/cm)	$5.411\cdot10^{5}$	–	$6.497\cdot10^{5}$
$k_{CH\text{-}CN}$ (dyn/cm)		–	$0.413\cdot10^{5}$
k_{CN} (dyn/cm)	$8.34\cdot10^{5}$	$12.53\cdot10^{5}$	$10.91\cdot10^{5}$
$k_{CN\text{-}NN}$ (dyn/cm)	$1.23\cdot10^{5}$	–	$1.95\cdot10^{5}$
k_{NN} (dyn/cm)	$16.89\cdot10^{5}$	$17.48\cdot10^{5}$	$18.98\cdot10^{5}$

[a] Unless otherwise indicated, Ref. [24].
[b] Cox, Thomas and Sheridan, cited in Ref. [24].

for which they find 1.189 Å and for k_θ which is a factor of 6 in error ($3.6\ 10^{-11}$ erg/rad^2). These rather large discrepancies show that equilibrium properties derived from very small basis set calculations should be considered as approximative only as some of the parameters thus calculated may be quite doubtful.

3.2. Dissociation Paths

3.2.1. Diabatic Potential Energy Surfaces

In Table 6, the "equilibrium" values of θ_{HCH} and R_{NN} are given along the dissociation paths of the four states considered. These values were derived from quadratic expressions in these parameters at each R_{CN} value considered.

The last row of Table 6 gives the calculated equilibrium angles of the corresponding four states of CH_2[5] and the equilibrium distance of N_2. These values are in fair agreement with the most precise values available in the literature: $R_{NN}^{eq}(\text{exp}) = 2.067$ a.u. [8];

Table 6. Dissociation path coordinates on diabatic potential energy surfaces (R in a.u.)

State	$^1A_1$		$^1A_1^*$		$^3B_1$		$^1B_1$	
R_{CN} \ θ, R_{NN}	θ°	R_{NN}	θ°	R_{NN}	θ°	R_{NN}	θ°	R_{NN}
2.435	122.6	2.170	–	–	–	–	–	–
3.2	146	2.094	92	2.117	119	2.111	132	2.115
4.1	165	2.080	102	2.095	129	(2.091)	141	(2.094)
5.0	177	2.081	106	2.087	132	2.082	(145)	2.083
∞	180	2.082	106	2.082	132	2.082	149	2.082

[5] Since the $^1A_1$ state of CH_2N_2 dissociates diabatically to $CH_2(^1A_1^*) + N_2(^1\Sigma_g^+)$, and the $^1A_1^*$ state to $CH_2(^1A_1) + N_2(^1\Sigma_g^+)$ (see Sect. 2.2), it follows that, at $R_{CN}\to\infty$, the first column of Table 6 refers to $CH_2(^1A_1^*)$ and the second to $CH_2(^1A_1)$.

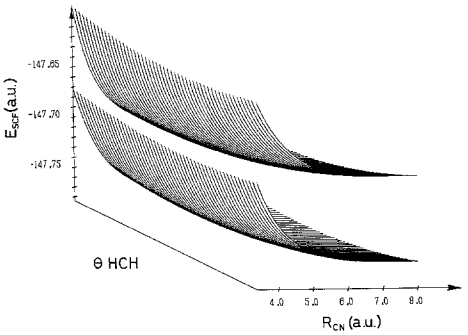

Fig. 2. SCF potential energy surfaces of $^3B_1$ and $^1B_1$ states (R_{NN} = 2.09 a.u., R_{CH} = 2.0385 a.u.). θ_{HCH} ranges from 100° (front) to 150° (back) with a 1° increment between curves

$\theta^{eq}_{HCH}(^1A_1)$(exp) = 102° [26]; $\theta^{eq}_{HCH}(^1A_1^*)$(calc) = 180° [7]; $\theta^{eq}_{HCH}(^3B_1)$(exp) = 136° [27]; $\theta^{eq}_{HCH}(^1B_1)$(exp) = 140 ± 15° [27].

The "equilibrium" values of R_{CH}, not listed in Table 6 show very little variation as a function of R_{CN}: according to the present findings, $R^{eq}_{CH}(^1A_1, CH_2N_2)$ = 2.04 a.u., whereas in CH_2 $R^{eq}_{CH}(^1A_1, ^1A_1^*, ^3B_1, ^1B_1)$ = 2.10, 2.00, 2.06, 2.03 a.u. respectively.

Furthermore, since the force constant k_{CH} is rather small ($\approx \frac{1}{3}k_{NN}$), the optimization of the energy with respect to this parameter gives rise to very small increments: using points 14, 19 and 20 of Table 3, one finds for instance that at R_{CN} = 5.0 a.u., the lowering of energy due to R_{CH} optimization is $\sim 5 \cdot 10^{-5}$ a.u. for the $^1A_1$ state. For this reason, the dissociation paths were not fully optimized with respect to R_{CH}, contrary to what was done for R_{NN} and θ_{HCH}.

Three-dimensional representations (E *vs.* R_{CN} *vs.* θ_{HCH}) are shown in Figs. 2 and 3.

3.2.2. CI Calculations

In Fig. 3, the locus of the crossing points of the two $^1A_1$ states is shown by a dashed line. 2 x 2 CI calculations were carried out to determine the interaction between these two states, and thus the adiabatic $^1A_1$ dissociation path.

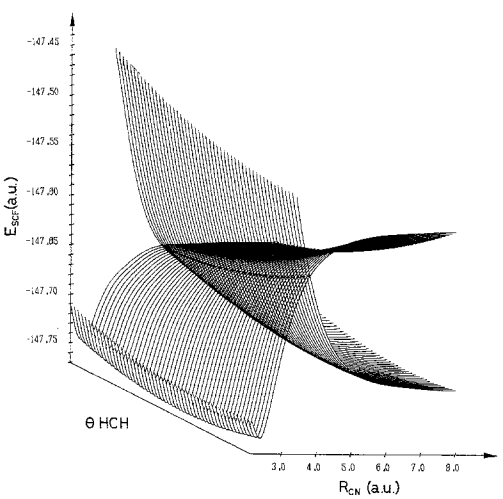

Fig. 3. SCF potential energy surfaces of $^1A_1$ and $^1A_1^*$ states (R_{NN} = 2.248 a.u., R_{CH} = 2.0385 a.u.). θ_{HCH} ranges from 100° (front) to 150° (back) with a 1° increment between curves. The locus of intersection points is shown by a dotted line

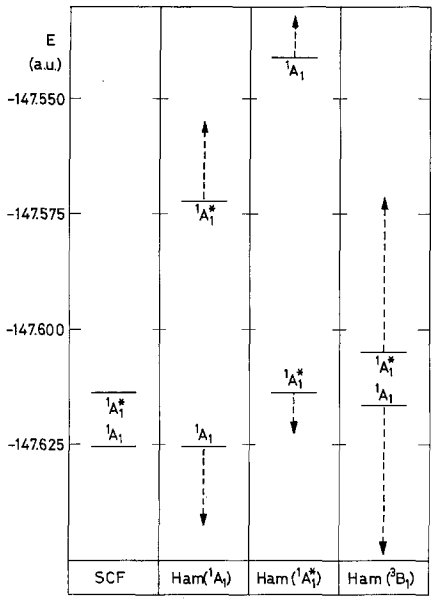

Fig. 4. CI (2 x 2) calculation between $^1A_1$ and $^1A_1^*$ states using different Hamiltonians. Left-hand column gives SCF energies. Dashed arrows indicate shifts in energy resulting from CI calculation. See text for more detail

The CI calculations envisaged here involve two configurations (B and C) which differ by the outermost orbitals: $\ldots(8a_1)^2$ and $\ldots(2b_1)^2$ for the $^1A_1^*$ and $^1A_1$ states respectively. The interaction term between the two states is thus the exchange integral $K_{8a_1 2b_1}$. Since $8a_1$ is a virtual orbital for Hamiltonian C and $2b_1$ for Hamiltonian B, it is apparent that neither of these Hamiltonians will describe the interaction term adequately. In addition, for the same reason, Hamiltonian B will give a poor energy for the $^1A_1$ state, as Hamiltonian C for the $^1A_1^*$ state.

Oppositely, in configuration A, corresponding to the $^3B_1$ state both orbitals $8a_1$ and $2b_1$ are occupied. Therefore, if use is made of Hamiltonian A, the deficiencies of Hamiltonians B and C should disappear to a large extent. Use of intermediate Hamiltonians, such as Hamiltonian A in this case, has been made previously by Salem, Leforestier, Segal and Wetmore [28].

Fig. 4 illustrates the importance of the choice of Hamiltonian on the CI result. It is noteworthy to point out that Hamiltonian A introduces an *absolute* error of $9 \cdot 10^{-3}$ a.u. in the energies of the two states considered, and, more important in a CI context, a *relative* error of $5 \cdot 10^{-4}$ a.u. only. Furthermore, numerous tests showed that the locus of intersection points of the two $^1A_1$ states was not altered by the change in Hamiltonian - Fig. 5 shows an example of this.

For these reasons, Hamiltonian A was used to calculate the energy displacements (ΔE_{CI}) of the two intersecting states. These energy increments were then added to the proper SCF energies in order to eliminate the absolute errors mentioned above. The numerical values of ΔE_{CI} are given in the last column of Tables 3 and 4.

3.2.3. Adiabatic Potential Energy Surfaces of the ^1A States

Fig. 7 shows the adiabatic surfaces of the two $^1A_1$ states. In Fig. 6 a more detailed description of the interaction is shown for one value of θ_{HCH}; for the sake of completeness, the SCF energies of the $^3B_1$ and $^1B_1$ states are also shown in this figure.

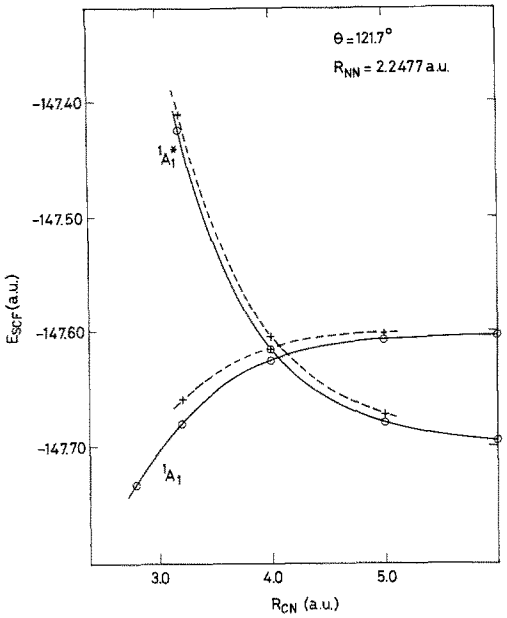

Fig. 5. Determination of intersection point of $^1A_1$ with $^1A_1^*$. Open circles and full lines: separate SCF calculations on both states. Crosses and dashed lines: common SCF calculation using $^3B_1$ Hamiltonian

The most relevant features in Figs. 6 and 7 are:

(1) the interaction between the two states is important and subsists as $R_{CN} \to \infty$;
(2) in spite of this "strong" interaction a potential barrier remains decreasing in importance as θ_{HCH} varies from 100–150°;
(3) at $R_{CN} \approx 4.35$ a.u. the energy is virtually independent of θ_{HCH}.

At all C-N interatomic distances considered here, the MO's $8a_1$ and $2b_1$ are both centered (almost exclusively) on CH_2, more particularly they correspond predominantly to carbon $2p_z$ and $2p_x$ AO's respectively. The fact that these two orbitals are centered in the same region of space explains why the integral $K_{8a_1 2b_1}$ is quite large at all R_{CN} values.

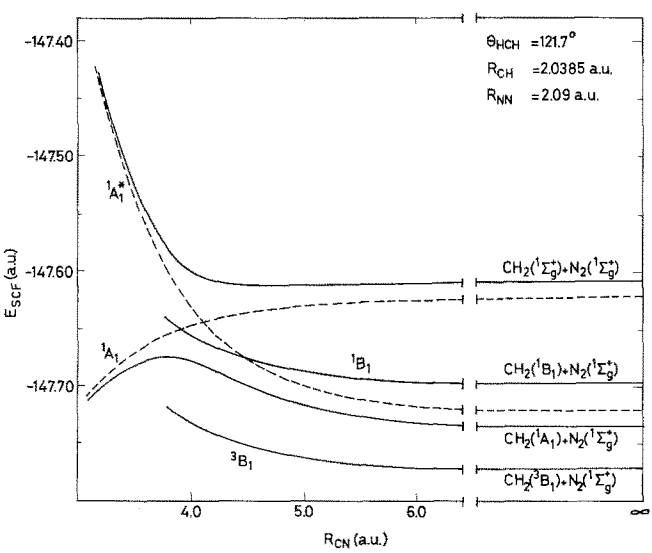

Fig. 6. Cross-section (R_{NN} = 2.09 a.u., θ_{HCH} = 121.7°) in potential surfaces showing calculated avoided crossing of the two $^1A_1$ states

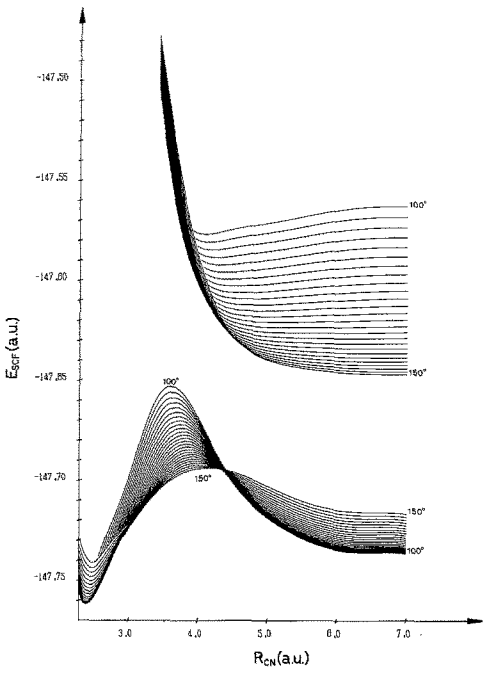

Fig. 7. Potential energy surfaces of the adiabatic $^1A_1$ and $^1A_1^*$ states (R_{NN} = 2.09 a.u., R_{CH} = 2.0385 a.u.) viewed from a direction parallel to the θ_{HCH} axis. θ_{HCH} varies from 100° to 150° with a 2° increment between curves

It is also for this reason that the potential barrier decreases as θ_{HCH} increases. Indeed, in the limiting case of $\theta_{HCH} = 180°$ (not calculated here), no barrier should subsist since the two diabatic surfaces do not intersect but rather merge to a common dissociation limit:

$$E^{SCF}(N_2, {}^1\Sigma_g^+) + \tfrac{1}{2}E^{SCF}(CH_2, {}^1\Sigma_g^+) + \tfrac{1}{2}E^{SCF}(CH_2, {}^1\Delta_g)^6.$$

The presence of the potential barrier is not surprising owing to the fact that, as mentioned above, the dissociation process limited to point group C_{2v} symmetries is not favoured by the Woodward-Hoffmann rules since the *adiabatic* dissociation path involves a change of symmetry of the outermost orbital ($2b_1 \rightarrow 8a_1$). According to these rules the lowest adiabatic dissociation path involves the molecule in a point group of lower symmetry in which C_{2v} irreducible representations b_1 and a_1 both correlate to the same irreducible representation. This point group is either C_S in which the plane σ bisects the H-C-H angle - this symmetry is achieved by variation of two additional parameters; out of plane $\theta_{N\text{-}C\text{-}H_2}$ and $\theta_{N\text{-}N\text{-}CH_2}$ - or C_1 in which all parameters are varied.

It is expected that in these groups, most, if not all of the potential energy maximum will disappear in agreement with experimental findings [26].

Fig. 7 makes it possible to visualize the adiabatic dissociation path as a function of θ_{HCH} in the limiting case of point group C_{2v}: for $2.4 < R_{CN} < 3.3$, the θ_{HCH} value

---

[6] Since the two states become degenerate as $R_{CN} \rightarrow \infty$, it follows that $\Delta E_{CI} = \pm K_{8a_1 2b_1}$. Furthermore as $R_{CN} \rightarrow \infty$, and $\theta_{HCH} \rightarrow 180°$, $K_{8a_1 2b_1}(CH_2N_2) \rightarrow K_{1\pi_{ux}1\pi_{uy}}(CH_2)$. It may be shown that if $1\pi_{ux} = 2p_x(C)$ and $1\pi_{uy} = 2p_y(C)$, one has $K_{1\pi_{ux}1\pi_{uy}} = \frac{1}{2}J_{1\pi_{ux}1\pi_{ux}} - \frac{1}{2}J_{1\pi_{ux}1\pi_{uy}} = \frac{1}{2}J^2_{1\pi_u 1\pi_u}$. Thus, since $\Delta E_{CI} = \pm \frac{1}{2}J^2_{1\pi_u 1\pi_u}$ and since in the SCF approximation $\Delta E^{SCF}(CH_2, {}^1\Sigma_g^+ - {}^1\Delta_g) = J^2_{1\pi_u 1\pi_u}$, it is normal that the common dissociation limit above lies halfway between the two "proper" dissociation products. In CH_2, the usual coordinate convention is adopted: in point group C_{2v}, the Z axis bisects the molecular angle and the X axis is perpendicular to the molecular plane; in point group $D_{\infty h}$, the Z axis is co-linear to the molecular axis.

increases from ~120° (equilibrium value of CH_2N_2, $^1A_1$) to 150°; for $3.3 < R_{CN} < 4.3$, the θ_{HCH} value increases further and probably reaches 170° (see diabatic path in Table 6); at $R_{CN} = 4.35$, there is a spectacular change in the value of θ_{HCH} going from ~170° to ~100°, the value of the energy being virtually independent of the angle at this distance; for $R_{CN} > 4.35$, the value of θ_{HCH} stays constant at 106° (equilibrium value of CH_2, $^1A_1$).

The height of the potential barrier may be estimated by the difference in energy at $R_{CN} = 4.35$ a.u. and the energy at $R_{CN} \to \infty$. We find 0.045 a.u. $\approx$ 1.2 eV. This rather high value means that the true dissociation path involves geometries which are probably quite distant from a C_{2v} conformation.

3.3. Population Analyses

The changes in electronic structure which occur as the molecule dissociates were analysed using Mulliken populations [21].

In Table 7 gross and overlap populations are given for $CH_2N_2(^1A_1)$ and for its diabatic dissociation products: $CH_2(^1A_1^*)$ and $N_2(^1\Sigma_g^+)$.

It is worth noting that the overall effect of the formation of the C-N_1 bond is very slight and results in a gross transfer of only 0.06 charge from CH_2 to N_2. The analysis of this overall effect shows, however, that this small charge results from much greater variations in the orbitals of different symmetry: in the a_1 orbitals there is a 0.7 charge transfer from N_2 to CH_2, in the b_1 orbitals there is a 0.7 charge transfer in the other direction, while in the b_2 orbitals there is a 0.4 charge transfer between the two N atoms balancing the charge differences introduced by the above a_1 and b_1 transfers.

The total overlap populations show, as expected, strong bonding characteristics between first neighbours and small anti-bonding characteristics between second neighbours. Comparison between the molecule and its dissociation products shows that the large charge density

Table 7. Gross and overlap populations of $CH_2N_2(^1A_1)$, $CH_2(^1A_1^*)$ and $N_2(^1\Sigma_g^+)$ ($\theta_{HCH} = 121.7$, $R_{CH} = 2.0385$, $R_{CN} = 2.423$, $R_{NN} = 2.148$)

Molecule (State)	Center	Sym. a_1	Sym. b_2	Sym. b_1	Total
$CH_2N_2(^1A_1)$	H	0.36	0.42	0	0.78
	C	3.97	1.10	1.31	6.38
	N_1	4.41	1.40	1.22	7.03
	N_2	4.90	0.66	1.47	7.03
	H-C	0.35	0.39	0	0.74
	C-N_1	0.66	−0.23	0.37	0.80
	N_1-N_2	0.27	0.46	0.16	0.89
	H-N_1	−0.02	0	0	−0.02
	C-N_2	−0.11	−0.04	−0.14	−0.29
	H_1-H_2	0.04	−0.06	0	−0.02
	H-N_2	0.01	0	0	0.01
$CH_2(^1A_1^*)$	H	0.28	0.47	0	0.75
	C	3.44	1.06	2.00	6.50
	H-C	0.33	0.39	0	0.72
	H_1-H_2	0.02	−0.09	0	−0.07
$N_2(^1\Sigma_g^+)$	N	5.00	1.00	1.00	7.00
	N-N	0.11	0.47	0.47	1.05

between C and N_1 results from the weakening of the N_1-N_2 bond, the rest of the charge coming from the net populations on C and N_1. It is noteworthy that the C-H bonds are not affected upon molecular formation.

In Fig. 8 the first-neighbour overlap populations of the $^1A_1$, $^1A_1^*$ and $^3B_1$ states are plotted as a function of R_{CN}. Among the different populations, only those of C-N for the $^1A_1^*$ and $^3B_1$ states are negative for all R_{CN} values considered; this is consistent with the repulsive nature of these two states.

The populations show that the anti-bonding nature of the C-N bond for these states is due almost exclusively to the MO $8a_1$, singly occupied in the $^3B_1$ state, and doubly occupied in the $^1A_1^*$ state, whence its strongly repulsive nature. The orbital $8a_1$ corresponds almost completely to a $2p_z$ orbital on the carbon atom; in CH_2, the corresponding orbital ($3a_1$) is a non-bonding lone pair with respect to the C-H bonds.

Since in point group C_{2v}, this lone pair is precisely the point of attack of the N_2 molecule, it follows that this orbital becomes strongly anti-bonding with respect to the C-N bond. It is interesting to note that, if the angle of approach of N_2 is modified (out of plane $\theta_{N\text{-}C\text{-}H_2} \neq 180°$), the repulsive nature of the diabatic $^1A_1^*$ state of CH_2N_2 is greatly reduced. Preliminary small-basis set calculations show that the optimum value of out-of-plane $\theta_{N\text{-}C\text{-}H_2}$ is roughly 90° at $R_{CN} = 3.8$ a.u. [5].

One has an inverse situation for $CH_2(^1\Sigma_g^+) + N_2(^1\Sigma_g^+)$. In this case the outermost orbital of $CH_2(1\pi_u)$ corresponds to a $2p_x \pm i2p_y$ charge density on the carbon atom. As N_2 approaches the carbon atom, the cylindrical $2p_x$, $2p_y$ charge density is destroyed, the CH_2 molecule bends and the outermost orbital of the resulting $^1A_1^*$ state ($1b_1$) corresponds now to a $2p_x$ charge density above and below the molecular plane. The N_2 point of attack according to group C_{2v} symmetry is then, in this case, the most favourable. Accordingly, the resulting CH_2N_2 state ($^1A_1$) is bonding.

In Fig. 8, one may also notice that for $R_{CN} < 3.2$ a.u. the N-N overlap population of the $^1A_1^*$ state becomes negative. This is due to the very repulsive nature of this state: at $R_{CN} = 3.2$ a.u. the dissociation channel: $CH_2N_2 \rightarrow CH_2N + N$ is opened.

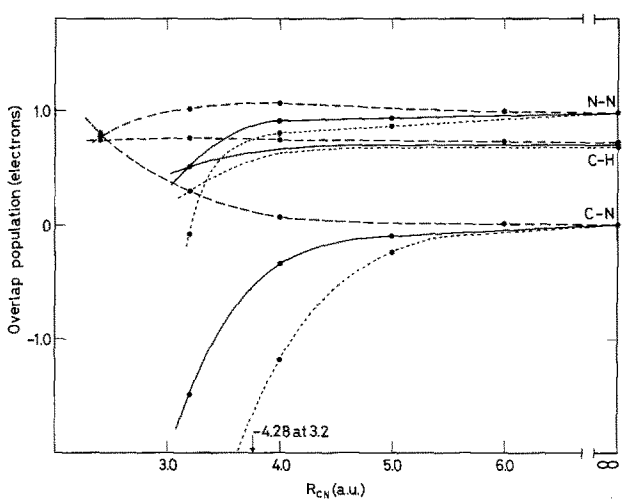

Fig. 8. Mulliken overlap populations for N-N, C-H and C-N bonds at $\theta_{HCH} = 121.7°$, $R_{NN} = 2.248$ and $R_{CH} = 2.0385$ a.u. Full lines refer to the $^3B_1$ state, dashed lines to the diabatic $^1A_1$ state and dotted lines to the diabatic $^1A_1^*$ state

Table 8. Data to calculate the dissociation energy of $CH_2N_2(^1A_1)$ and the term energy of $CH_2(^1A_1)$[a]

Energy (a.u.)	$CH_2N_2(^1A_1)$	$N_2(^1\Sigma_g^+)$	$CH_2(^3B_1)$	$CH_2(^1A_1)$
SCF[b]	−147.821	−108.926	−38.911	−38.874
Correlation	− 0.781	− 0.501	− 0.221	− 0.240
Total	−148.602	−109.427	−39.132	−39.114

[a] Energies calculated at equilibrium geometries (basis set VII): CH_2N_2, see Table 5; N_2, R_{NN} = 2.082 a.u.; $CH_2(^3B_1)$, $\theta = 132°$, R_{CH} = 2.039 a.u.; $CH_2(^1A_1)$, $\theta = 106°$, R_{CH} = 2.1 a.u.

[b] Basis set X.

3.4. Dissociation Energy

The dissociation energy of CH_2N_2 was calculated from the best available SCF energies (basis set X) together with estimated correlation energies (see Sect. 2.6). These energies are given in Table 8.

The last two columns of Table 8 show that the difference in correlation energy between the $^3B_1$ and $^1A_1$ states of CH_2 is 0.019 a.u. According to population analyses, the MO's $3a_1$ and $1b_1$, which are the outermost orbitals of these states ($^3B_1$: ... $3a_1 1b_1$; $^1A_1$: ... $3a_1^2$), correspond almost exclusively respectively to $2p_z$ and $2p_x$ orbitals on the carbon atom.

Thus one has the approximate equivalence:

$$E^{CORR}(CH_2, {}^3B_1) - E^{CORR}(CH_2, {}^1A_1) \approx E^{CORR}(C, {}^3P) - \tfrac{1}{3}E^{CORR}(C, {}^1S) - \tfrac{2}{3}E^{CORR}(C, {}^1D) = 0.020 \text{ a.u. [22]},$$

in agreement with the molecular value.

From the total energies of Table 8, we calculate:

$$D_e(CH_2N_2, (^1A_1) \rightarrow CH_2(^1A_1) + N_2(^1\Sigma_g^+)) = 0.061 \text{ a.u.} = 1.66 \text{ eV},$$

as the adiabatic dissociation energy.

In order to calculate the "thermodynamic" dissociation energy, zero-point energies have to be considered. To this end, the vibration frequencies of *gaseous* CH_2N_2 were taken from the work of Moore and Pimentel [24], that of N_2 from the Rosen tables [29], while for the CH_2 frequencies, by default of experimental values, we adopted the theoretical values of O'Neil, Schaeffer and Bender [30] which were obtained from correlated wave-functions. These values, combined with the appropriate energies of Table 8, yield:

$$D_0^0(CH_2N_2(^1A_1) \rightarrow CH_2(^3B_1) + N_2(^1\Sigma_g^+)) = 0.91 \text{ eV} = 21 \text{ kcal/mole}.$$

This result may be compared with a few existing experimental upper limits:

photodissociation measurements:	<41.7 kcal/mole	[31]
electron impact:	<44 kcal/mole	[32]
pyrolysis:	<35 kcal/mole	[33]

Also, Braun, Bass and Pilling [34] cite a value of 25 kcal/mole. The only theoretical values are those of Leroy and Sana [4], who find:

$$\Delta H_0^0 \text{ (formation)} = 58.85 \text{ kcal/mole}$$

These authors [4] also cite values of 61.03 and 62.83 kcal/mole from consideration of isodesmic reactions [35]. The resulting dissociation energies (D_0^0) range from 29 to 33 kcal/mole in fair agreement with our value.

3.5. *Term Value of* $CH_2(^1A_1)$

The controversial term energy of the $^1A_1$ state of CH_2 may also be calculated from the data of Table 8. We find:

$$T_e(^1A_1) = 0.49 \text{ eV} = 11 \text{ kcal/mole}.$$

There are a large number of calculated values for this property. Most of these predict a term value of ~1 eV. It is only the most recent large-scale SCF-CI calculations carried out with basis sets including polarization functions which give values systematically lower: Hay, Hunt and Goddard III [36] find 0.50 eV; Staemmler [37] finds 0.38 eV, and Handy [38] finds 0.67 eV.

Experimentally, the situation is not clear. There exist measurements which indicate a very low term value: 1-2.4 kcal/mole [39]. Oppositely other measurements lead to a higher term value 8-9 kcal/mole [40]. Spectroscopically, Herzberg and Johns [27] find an upper limit of ~1 eV.

Finally, Harrison [41] in a recent article reviewing all previous experimental and theoretical determinations favours a value of 9-10 kcal/mole (~0.4 eV). Our result is in satisfactory agreement with this value considering that our basis set is only of *DZ+* polarization quality and considering the approximation made here for the determination of the corellation energies.

4. Conclusions

In this work we have investigated the dissociation behaviour of CH_2N_2 into CH_2 and N_2 products in the limiting case of point group C_{2v} symmetries.

Most of the results given above should be quite reliable. They concern the equilibrium geometry, the dissociation energy and the $CH_2(^1A_1)$ term value. In this list we may also include the electronic rearrangements discussed in Sect. 3.3.

The major uncertainties remaining concern the height of the potential barrier in the lower $^1A_1$ state. Different contributions to this quantity, such as: influence of basis set, correlation energy and differences in zero-point energies, might influence notably the height of the barrier. It is probable that the first factor will increase slightly the height of the barrier, whereas the latter two will decrease it considerably.

No quantitative estimates of these factors have been made, however, since according to the Woodward-Hoffmann rules the C_{2v} dissociation path is not expected to be the lowest. Indeed preliminary calculations with smaller basis sets show that at intermediate R_{CN} values, lower energies are obtained for non-planar conformations of the molecule. The result of these calculations will be reported in a forthcoming paper.

Acknowledgements. The authors thank M. D. Gervy and Y. Gaudy for help in some of the calculations, Professor G. Leroy and Dr. M. Sana for useful discussion, and are particularly grateful to Professor J. L. Whitten for his programmes. They acknowledge support from the Brussels University

Computing Center. Financial support was also given to one of us (G. V.) through research grants of the Fonds de la Recherche Fondamentale Collective (FRFC, Belgium) and of the NATO Science Committee.

References

1. See e.g.: Allinger, N. L., Cava, M. P., De Jongh, D. C., Johnson, C. R., Lebel, N. A., Stevens, C. L.: Organic chemistry. New York, N.Y.: Worth Publishers 1971
2. Snyder, L. C., Basch, H.: J. Am. Chem. Soc. **91**, 2189 (1969)
3. Hart, B. T.: Aust. J. Chem. **26**, 461, 477 (1973)
4. Leroy, G., Sana, M.: Theoret. Chim. Acta (Berl.) **33**, 329 (1974)
5. Lievin, J., Verhaegen, G.: to be published
6. Woodward, R. B., Hoffmann, R.: The conservation of orbital symmetry. Weinheim: Verlag Chemie 1970
7. Chu, S. Y., Siu, A. K. Q., Hayes, E. F.: J. Am. Chem. Soc. **94**, 2969 (1972)
8. Herzberg, G.: Spectra of diatomic molecules. Princeton, New Jersey: Van Nostrand 1950
9. Hehre, W. J., Stewart, R. F., Pople, J. A.: J. Chem. Phys. **51**, 2657 (1969)
10. Clementi, E.: J. Chem. Phys. **46**, 4737 (1967)
11. Burden, F. R., Hart, B. T.: Aust. J. Chem. **26**, 1395 (1973)
12. Ditchfield, R., Hehre, W. J., Pople, J. A.: J. Chem. Phys. **54**, 724 (1971)
13. Whitten, J. L.: J. Chem. Phys. **44**, 359 (1966)
14. Huzinaga, S.: J. Chem. Phys. **42**, 1293 (1965)
15. Whitten, J. L.: J. Chem. Phys. **39**, 349 (1963)
16. Whitten, J. L.: Hackmeyer, M.: J. Chem. Phys. **51**, 5584 (1969)
17. Whitten, J. L.: J. Chem. Phys. **56**, 5458 (1972)
18. Basch, H., Robin, M. B., Kuebler, N. A.: J. Chem. Phys. **47**, 1201 (1967)
19. Williamson, H.: C.A.C.M. **15**, 100 (1972)
20. Liu, H. P. D., Verhaegen, G.: J. Chem. Phys. **53**, 735 (1970); Int. J. Quantum Chem. **5**, 103 (1971)
21. Mulliken, R. S.: J. Chem. Phys. **23**, 1833 (1955)
22. Verhaegen, G., Moser, C. M.: J. Phys. B: Atom. Mol. Phys. **3**, 478 (1970)
23. Desclaux, J. P., Moser, C. M., Verhaegen, G.: J. Phys. B: Atom. Molec. Phys. **4**, 296 (1971)
24. Moore, C. B., Pimentel, G. C.: J. Chem. Phys. **40**, 329, 342 (1964)
25. Cox, A. P., Thomas, L. F., Sheridan, J.: Nature (London) **181**, 1000 (1958)
26. Wasserman, E., Hutton, R. S., Kuck, V. J., Jager, W. A.: J. Chem. Phys. **55**, 2593 (1971)
27. Herzberg, G., Johns, J. W. C.: J. Chem. Phys. **54**, 2276 (1971)
28. Salem, L., Leforestier, C., Segal, G., Wetmore, R.: J. Am. Chem. Soc. **97**, 479 (1975)
29. Selected constants. Spectroscopic data relative to diatomic molecule, Rosen, B. Ed. Oxford: Pergamon Press 1970
30. O'Neil, S., Schaeffer III, H. F., Bender, C. F.: J. Chem. Phys. **55**, 162 (1971)
31. Laufer, A. H., Okabe, H.: J. Am. Chem. Soc. **93**, 4137 (1971)
32. Paulett, G. S., Ettinger, R.: J. Chem. Phys. **39**, 825, 3534 (1963)
33. Setser, D. W., Rabinovitch, B. S.: Can. J. Chem. **40**, 1425 (1962)
34. Braun, W., Bass, A. M., Pilling, M.: J. Chem. Phys. **52**, 5131 (1970)
35. For definition of method see: Hehre, W. J., Ditchfield, R., Radom, R., Pople, J. A.: J. Am. Chem. Soc. **92**, 4796 (1970)
36. Hay, P. J., Hunt, W. J., Goddard III, W. A.: Chem. Phys. Letters **13**, 30 (1972)
37. Staemmler, V.: Theoret. Chim. Acta (Berl.) **31**, 49 (1973)
38. Handy, N. C.: Communication at the Seminar on Computational Methods in Molecular Physics, Strasbourg, September 1975
39. Halberstadt, M. L., McNesby, J. R.: J. Am. Chem. Phys. **89**, 4317 (1967); Carr Jr., R. W., Eder, T. W., Toper, M. G.: J. Chem. Phys. **53**, 5716 (1970)
40. Frey, H. M.: J. Chem. Soc. Chem. Commun. 1024 (1972); Frey, H. M., Kennedy, G. J.: Chem. Commun. **6**, 233 (1975)
41. Harrison, J. F.: Accounts Chem. Res. **7**, 378 (1974)

Received December 22, 1975/February 16, 1976